The Astrophysical Journal, 569:1016–1025, 2002 April 20

CORRELATION OF THE CORONAL MASS EJECTION PRODUCTIVITY OF SOLAR ACTIVE REGIONS WITH MEASURES OF THEIR GLOBAL NONPOTENTIALITY FROM VECTOR MAGNETOGRAMS: BASELINE RESULTS

D. A. Falconer,[1] R. L. Moore, and G. A. Gary
Marshall Space Flight Center, SD50/Space Science Department, Huntsville, AL 35812;
david.falconer@msfc.nasa.gov, ron.moore@msfc.nasa.gov, allen.gary@msfc.nasa.gov
Received 2001 October 24; accepted 2001 December 10

ABSTRACT

From conventional magnetograms and chromospheric and coronal images, it is known qualitatively that the fastest coronal mass ejections (CMEs) are magnetic explosions from sunspot active regions in which the magnetic field is globally strongly sheared and twisted from its minimum-energy potential configuration. In this paper, we present measurements from active region vector magnetograms that begin to quantify the dependence of the CME productivity of an active region on the global nonpotentiality of its magnetic field. From each of 17 magnetograms of 12 bipolar active regions, we obtain a measure of the size of the active region (the magnetic flux content, Φ) and three different measures of the global nonpotentiality (L_{SS}, the length of strong-shear, strong-field main neutral line; I_N, the net electric current arching from one polarity to the other; and $\alpha = \mu I_N/\Phi$, a flux-normalized measure of the field twist). From these measurements and the observed CME productivity of the active regions, we find that: (1) All three measures of global nonpotentiality are statistically significantly correlated with each other and with the active region flux content. (2) All three measures of global nonpotentiality are significantly correlated with CME productivity. The flux content has some correlation with CME productivity, but at a less than statistically significant confidence level (less than 95%). (3) The net current is less strongly correlated with CME productivity than is α, and the correlation of flux content with CME productivity is weaker still. If these differences in correlation strength, and a significant correlation of α with flux content, persist to larger samples of active regions, this would suggest that active region size does not affect CME productivity except through global nonpotentiality. (4) For each of the four global magnetic quantities, the correlation with CME productivity is stronger for a ± 2 day time window for the CME production than for windows half as wide or twice as wide. This plausibly results from most CME-productive active regions producing less than one CME per day, and from active region evolution often significantly changing the global nonpotentiality over the course of several days. These results establish that measures of active region global nonpotentiality from vector magnetograms (such as L_{SS}, I_N, and α) should be useful for prediction of active region CMEs.

Subject headings: Sun: coronal mass ejections (CMEs) — Sun: magnetic fields — Sun: X-rays, gamma rays

1. INTRODUCTION

The fastest coronal mass ejections (CMEs) blast out through the corona and plow into the solar wind at speeds of $\sim 10^3$ km s^{-1}, driving a bow shock that accelerates protons and other ions to cosmic-ray energies of 100 MeV or more (Wagner 1984; Kahler 1987; Krimigis 1992; Gosling 1996; Reames 1999). Most of these come from explosions of the strong ($\geq$100 G) magnetic fields in active regions with sunspots, explosions that produce a flare in tandem with the CME and often begin with a filament eruption and flare spray (Rust et al. 1980; Tandberg-Hanssen, Martin, & Hanssen 1980; MacQueen & Fisher 1983; Sheeley et al. 1983; Moore 1988, 2001[2]). These events are the greatest explosions in the solar system; the strongest ones release $\sim 10^{32}$ ergs of magnetic energy in $\sim 10^3$ s, transiently far exceeding the global power input to the steady solar wind.

A CME produced by an active region near central meridian is directed more or less earthward, and, if massive enough, can be seen by a coronagraph at Earth as a halo CME (visible around the entire occulting disk). In Figure 1 is an image (from the Large Angle and Spectrometric Coronagraph Experiment [LASCO] of the *Solar and Heliospheric Observatory* [*SOHO*]) of a halo CME that was produced together with a large flare by an active region located 25° northeast of disk center. The 1–10^3 MeV particle radiation from a strong halo CME can be harmful or even lethal to communication satellites and astronauts outside the Earth's magnetosphere, and the magnetic storm wrought by the CME impacting the magnetosphere can knock out electrical power grids on the ground. So, in addition to the astrophysical importance of advancing our understanding of CMEs, there are considerable economic, safety, and security concerns that motivate the development of reliable methods of predicting active region explosions that produce strong earthward CMEs.

An active region is built by the emergence of bundles of magnetic flux loops from below the photosphere. The ensemble of emerged loops is usually grossly bipolar, roughly in the form of an Ω loop rooted in two adjacent areas of predominantly opposite polarity flux. The boundary between these two contiguous areas is the main neutral line (polarity dividing line), which runs through the middle of the active region. In the largest CME-producing explosions in active regions, such as in the great flares of 1972 August (Zirin & Tanaka 1973; Rust et al. 1980; Moore

[1] Physics Department, University of Alabama at Huntsville, Huntsville, AL 35899.
[2] Available at: http://www.ency-astro.com.

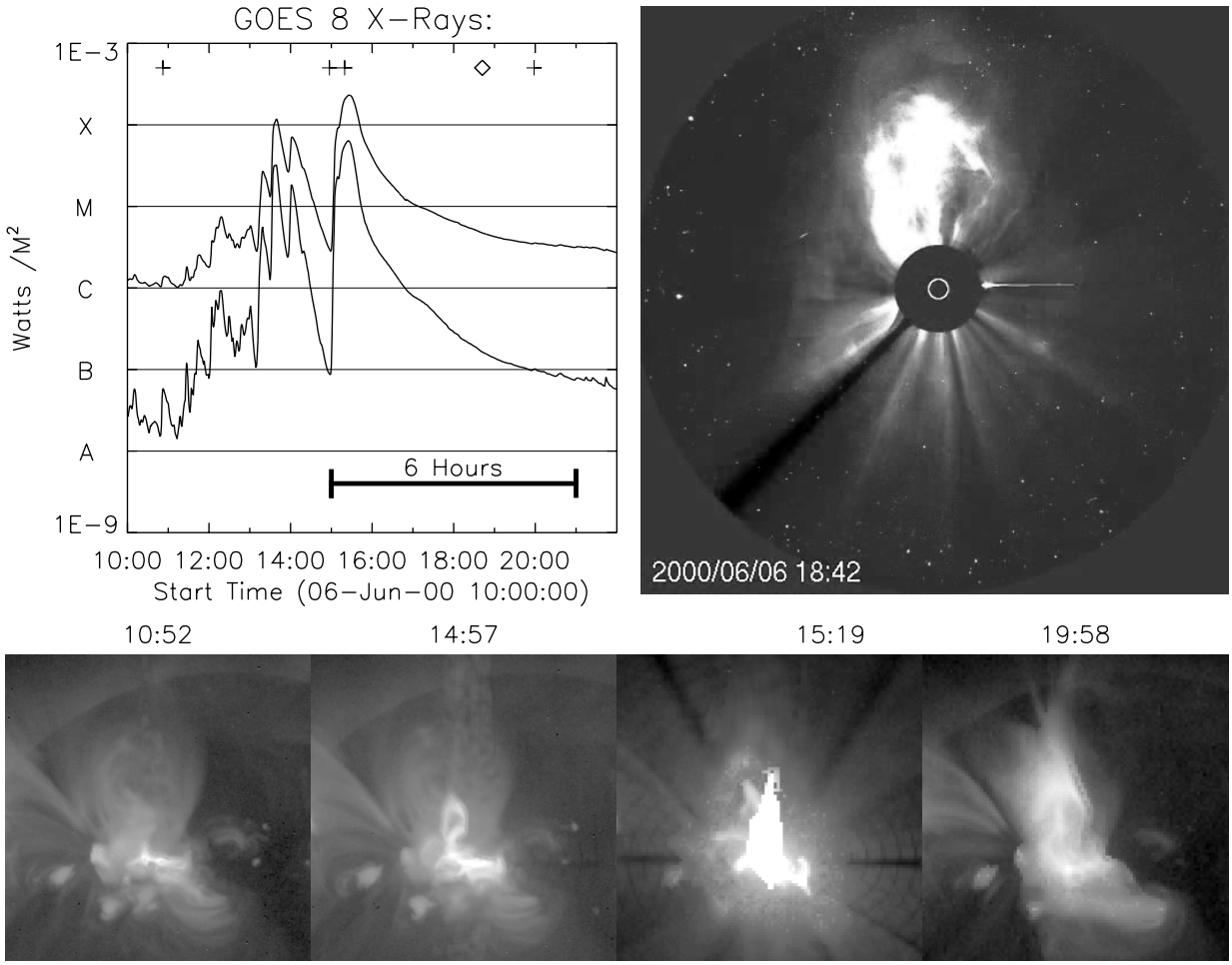

FIG. 1.—Reliable signatures of CMEs that erupt from active regions. *Top right*: *SOHO*/LASCO image of a halo CME on 2000 June 6 at 18:42 UT. The location and size of the solar disk are shown by the white circle centered in the shadow of the occulting disk. This CME was produced in conjunction with a long-duration *GOES* X-class flare in AR 9026, which was on the central part of the disk at 21° north, 14° east. In this image, the CME is seen as enhanced coronal brightness extending out for many solar radii beyond and around the entire circumference of the occulting disk. Because the active region explosion that produced the CME was offset from disk center to the northeast, and because a prior slow northward CME from the back side of the Sun was in progress and was overtaken (in projection along the line of sight) by the fast halo CME, by far the brightest ejecta in this image are in the sector east of north. *Bottom*: Sequence of four *Yohkoh* SXT X-ray images of the active region before and during the flare. The universal time of each image is above the image. The sequence shows the active region (1) near the onset of flaring activity that began in the active region a few hours before the long-duration flare, (2) at the onset of the rise phase of the long-duration flare, (3) near the peak of the flare, and (4) late in the long-duration decay phase of the flare. The decay-phase image shows a cusp-top arcade of late-phase flare loops, the typical signature indicating that the eruption produced a CME. *Top left*: *GOES* X-ray flux time profiles of the flare (*upper profile*, 1–8 Å flux; *lower profile*, 0.5–3 Å flux). The time of the CME image is marked by the diamond, and the time of each of the four X-ray images is marked by a plus sign.

1988) and in the example shown in Figures 1 and 2, the overall bipole explodes and the flare straddles the main neutral line. In these active regions, in chromospheric images, a filament and/or fibrils run along a channel tracing the main neutral line, showing that the core field of the bipole (the field rooted near the neutral line and closely enveloping it) is strongly sheared relative to its minimum-energy (potential) configuration. This shows that the core field has a large store of nonpotential magnetic energy that in principle is available for release in an explosion. If a filament traces the whole length of the main neutral line, the entire core field of the bipole is strongly nonpotential. In this case, because the sheared core field spans the active region, the active region is in this manner globally nonpotential (e.g., Antiochos et al. 1994; Moore et al. 1997). The eruption of these core-field–tracing filaments in large CME explosions indicates that the explosion is driven by release of nonpotential magnetic energy from the stressed core field, and suggests that this form of global nonpotentiality is a precondition for the explosion (Moore et al. 1987, 1991; Moore 1987, 1988; Moore & Roumeliotis 1992).

The longstanding implication from chromospheric filaments that globally sheared core fields are characteristic of CME-productive active regions has been corroborated and strengthened by coronal X-ray observations of active region magnetic structure. From coronal X-ray images from the *Yohkoh* soft X-ray telescope (SXT), Canfield et al. (1999) found that active regions with obvious sigmoids running through them are more likely to produce CMEs than are active regions showing no large-scale sigmoidal structure. The sigmoids are sinuous magnetic structures having the overall shape of an S or inverse S. In typical, grossly bipolar sigmoidal active regions, the middle of the S overlies and traces the main neutral line through the core of the overall magnetic bipole of the active region (e.g., Falconer et al. 2000; Moore et al. 1997). Thus, in essentially the same way

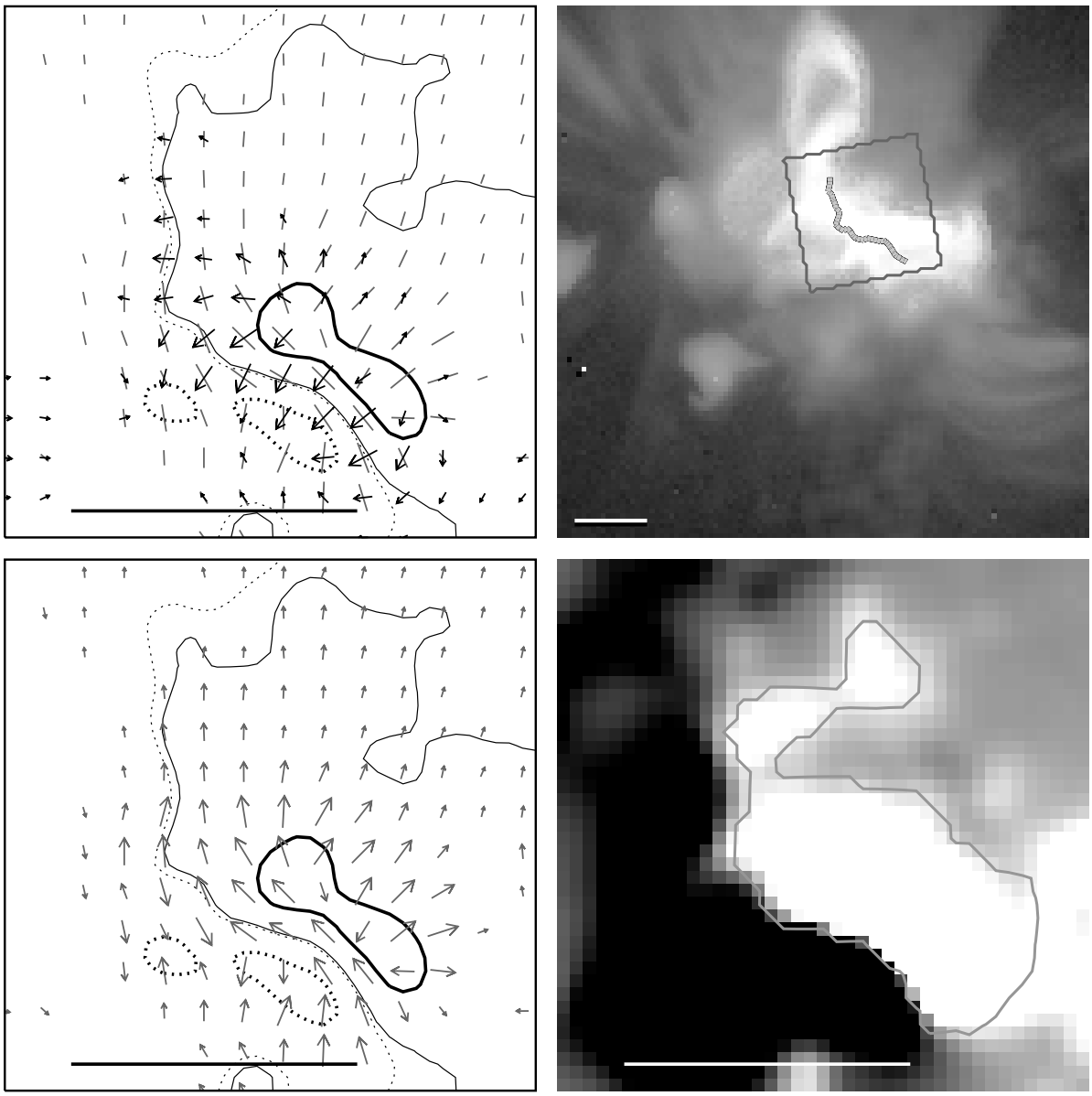

FIG. 2.—Vector magnetogram and elements of our method for extracting L_{SS} and I_N. This example is for AR 9026 on the day that it produced the CME shown in Fig. 1. *Top left*: Vector magnetogram with superposed transverse component (*arrows*) of the potential field. The field of view shown here, which covers the strong magnetic field in and around the main sunspots of this active region, is roughly the central quarter of the full magnetogram. The strength of the line-of-sight component of the observed field is mapped by the contours (25, 500 G; solid for positive polarity, dashed for negative polarity). The strength and orientation of the observed transverse component are mapped by the gray dashes for transverse field strengths from 150 G (*shortest dashes*) to $\geq$500 G (*longest dashes*). Likewise, the arrows display the potential field's transverse component where it is 150 G or stronger. *Top right*: Map (*gray path*) of the strong magnetic shear on the main neutral line, overlaid on a coronal X-ray image of the active region from *Yohkoh* SXT. The X-ray image is at the onset of the long-duration X-class flare and CME shown in Fig. 1 (north is up, west is right). The tilted square is the field of view of the magnetogram in the other three panels. The gray path traces only part of the main neutral line, the part on which the observed transverse field and the potential transverse field are both strong ($\geq$150 G) and the observed transverse field is strongly sheared (shear angle $\geq 45^\circ$). The length of this path is L_{SS}. *Bottom left*: The vector magnetogram after resolution of the 180° ambiguity in the direction of the transverse field. The gray arrows here are the same as the gray dashes in the raw vector magnetogram in the top left panel, but with the direction now assigned. *Bottom right*: Gray-scaled map of the line-of-sight component of the vector magnetogram (light for positive polarity, dark for negative polarity). The contour encircles all of the positive polarity domain in which the line-of-sight component is stronger than 100 G and the transverse component is stronger than 150 G. Integration of the direction-resolved transverse field around this contour gives the active region's net electric current inside the contour. This quantity is I_N. The bar in each panel is 50,000 km long.

as a filament running along the main neutral line, a sigmoid also shows that the core field is greatly sheared from its potential configuration, so that it runs nearly parallel to the neutral line rather than nearly perpendicular. The overall magnetic bipole of an obviously sigmoidal active region is decidedly globally nonpotential; the field displays large shear and twist of a single sense (right-handed for S shapes, left-handed for inverse-S shapes) on the scale of the whole bipole. Hence, as does a filament, a sigmoid traversing the main neutral line through an active region indicates that the active region has large global nonpotentiality and a corresponding large store of free magnetic energy available for CME production.

In addition to finding that sigmoidal active regions are more CME productive than nonsigmoidal active regions, Canfield et al. (1999) also found, for sigmoidal active

TABLE 1

MEASURED GLOBAL MAGNETIC QUANTITIES AND IDENTIFIED CME OCCURRENCES IN OUR ACTIVE REGIONS

No.	Date of Magnetogram	AR	Longitude[a] (deg)	Latitude (deg)	Φ (10^{21} Mx)	L_{SS} (10^3 km)	I_N (10^{11} A)	α (10^{-8} m^{-1})	Day of CME Relative to Day of Magnetogram
1.....	1991 Dec 26	6982	W18	S14	32 ± 6*	122 ± 25*	41 ± 8*	1.1 ± 0.3*	$-6, +2$
2.....	1992 Feb 27	7070	W8	N7	35 ± 7*	115 ± 23*	41 ± 8*	0.99 ± 0.3*	$-6, -3, 0, +7$
3.....	1992 Feb 28	7070	W21	N7	36 ± 7*	107 ± 22*	38 ± 8*	0.88 ± 0.3*	$-7, -4, -1, +6$
4.....	1992 Jul 12	7220	W10	S12	12 ± 2	25 ± 6	2 ± 1	0.15 ± 0.1	...
5.....	1992 Aug 16	7260	E20	N16	37 ± 7*	53 ± 12*	23 ± 5*	0.52 ± 0.2*	$+4$
6.....	1992 Oct 19	7315	E23	N7	7 ± 1	3 ± 3	1 ± 1	0.15 ± 0.1	...
7.....	1992 Oct 21	7315	W2	N5	17 ± 3	7 ± 6	3 ± 1	0.16 ± 0.1	...
8.....	1992 Oct 23	7315	W31	S6	25 ± 5*	42 ± 11	2 ± 1	0.05 ± 0.03	...
9.....	1996 Nov 27	7999	W17	S4	19 ± 4	47 ± 11	5 ± 2	0.23 ± 0.1	3
10.....	1997 Sep 7	8083	E6	S27	7 ± 1	18 ± 4	1 ± 1	0.11 ± 0.1	...
11.....	1997 Oct 31	8100	E21	S19	6 ± 1	$28 \pm$	1 ± 1	0.13 ± 0.1	4, 6, 7
12.....	1997 Nov 3	8100	W21	S19	14 ± 3	85 ± 17*	7 ± 2	0.44 ± 0.1*	0, 2, 3
13.....	1997 Nov 18	8108	E20	N21	12 ± 2	32 ± 7	13 ± 3*	0.90 ± 0.3*	$-4, -2, +1$
14.....	1998 Sep 2	8323	E2	S23	24 ± 5*	102 ± 21*	12 ± 3*	0.40 ± 0.1	...
15.....	2000 Jun 6	9026	E14	N21	26 ± 5*	146 ± 29*	32 ± 6*	1.0 ± 0.3*	$-3, 0, +1, +4$
16.....	2000 Jul 14	9077	W6	N17	38 ± 7*	218 ± 44*	38 ± 8*	0.84 ± 0.2*	$-4, -3, -2, 0$
17.....	2000 Jul 16	9077	W30	N18	20 ± 4*	179 ± 37*	34 ± 7*	1.4 ± 0.4*	$-6, -5, -3, -2$
Median...					20	53	12	0.44	

NOTE.—Asterisks denote measured values that are greater than or equal to the median.

[a] At 16:00 UT.

regions and for nonsigmoidal active regions, that CME productivity increases with active region size measured by sunspot area. That some nonsigmoidal active regions produce CMEs suggests that these might have as much global nonpotentiality as some sigmoidal active regions, but for some reason do not show recognizable sigmoidal structure in coronal images. That CME productivity increases with active region size suggests that the degree of global magnetic shear and twist may tend to be greater in larger active regions. To investigate these possibilities, active region global nonpotentiality needs to be assessed quantitatively and independently of whether the core field displays a chromospheric filament or coronal sigmoid.

Measures of the global nonpotentiality of an active region can be obtained from a vector magnetogram of the region regardless of the clarity of global magnetic shear or twist in chromospheric or coronal images. In a pilot study of four bipolar active regions, Falconer (2001) explored this quantitative approach to gauging global nonpotentiality for prediction of the CME productivity of active regions. The global magnetic shear was measured by the length of the portion of the main neutral line on which the field was strongly sheared, and the global magnetic twist was measured by the net electric current flowing from one polarity of the overall bipole to the other. Two of the four active regions had much larger measures of global magnetic shear and twist than did the other two. The two active regions having large measures of global nonpotentiality displayed obvious large-scale magnetic twist and/or shear in SXT coronal images, and each produced multiple CMEs during disk passage; whereas the two active regions having small measured global nonpotentiality appeared to be globally nearly potential in SXT images and produced no CMEs. Thus, the pilot study demonstrated that length of strong magnetic shear on the main neutral line and net current are both practical measures of active region global nonpotentiality that can be obtained from vector magnetograms, and tentatively indicated that both of these quantities are correlated with the CME productivity of active regions. That is, these two measurable quantities from vector magnetograms showed promise for usefulness in forecasting earthward CMEs.

The work reported in the present paper is an expansion and refinement of the Falconer (2001) pilot study. The pilot study was limited to eight vector magnetograms of four active regions. In the present study, we have expanded the sample to 17 magnetograms of 12 active regions (Table 1). This sample is large enough to allow a first look at the statistical significance of the correlation of the measured global magnetic quantities with each other and with the CME productivity of the active regions. The pilot study could not address the dependence of CME productivity on active region size because the four active regions were nearly the same size (within a factor of 2) in terms of their magnetic flux content. In the expanded sample, the active region flux content ranges over a factor of 6, allowing us to begin delving into whether active region CME productivity has a dependence on active region size in addition to its dependence on active region global nonpotentiality. We do this by checking whether CME productivity is more strongly correlated with the net current than with the net current normalized by active region size (net current divided by the flux content). For our active regions, we find to the contrary that the CME productivity is somewhat more strongly correlated with the flux-normalized net current than with the net current. That is, our present sample shows no evidence of CME productivity depending on active region size (flux content) independently of the global nonpotentiality. We do find that our four active region global magnetic quantities (magnetic flux content, strong-shear length of main neutral

line, net current, and flux-normalized net current) are all significantly correlated with each other, and that all but the flux content are significantly correlated with the CME productivity. This certifies (1) the tentative findings of the pilot study, and (2) that our four global magnetic quantities are worthy of further evaluation of their efficacy for CME prediction, through similar analysis of a larger sample of active regions.

2. DATA

The 17 vector magnetograms used in this study are from the Marshall Space Flight Center vector magnetograph (Hagyard et al. 1982; West et al. 2002). The date of each magnetogram and the active region observed in the magnetogram are given in Table 1. This set of active region vector magnetograms includes 7 of the 8 magnetograms used in the Falconer (2001) pilot study of four active regions, together with 10 magnetograms of eight additional active regions. These active regions and their magnetograms were selected by the following criteria. First, we selected only high-quality magnetograms that were obtained under acceptably good seeing conditions. Second, we required that on the day of the magnetogram the active region was within 30° of central meridian, so that the active region was viewed fairly well face-on. In the present study, foreshortening and other projection effects are neglected. That is, the active region global magnetic quantities are measured in the image plane. Third, we required that each active region was predominantly bipolar, i.e., had an obvious main neutral line. Finally, we selected only active regions that occurred during the *Yohkoh* mission (1991 to present), so that each active region was monitored from limb to limb in coronal X-ray images from the *Yohkoh* SXT (Tsuneta et al. 1991) as the region rotated across the disk. As in Falconer (2001), we use some active region coronal magnetic structures (sigmoids and core-field strands) seen in the SXT images to determine the sense of strong magnetic shear across the main neutral line, and identify the occurrence or absence of other structures (cusped arcades) as evidence of whether the active region produced CMEs.

From each vector magnetogram, we measure three primary global magnetic quantities, which, singly or in combination, gauge the global nonpotentiality of the active region. These three quantities are (1) L_{SS}, the length of strong magnetic shear on the main neutral line, (2) I_N, the net electric current flowing up or down in one polarity half of the overall bipole, and (3) Φ, the magnetic flux content of the active region. The net current normalized by the flux content (I_N/Φ) amounts to a global gauge of the severity of the twist in the magnetic field, independent of the size of the active region, because I_N/Φ sets the value of the twist parameter $\alpha = \mu I_N/\Phi$, where μ is the permeability of free space. From Ampere 's law ($\nabla \times \boldsymbol{B} = \mu \boldsymbol{J}$), the quantity α is a characteristic value of $|\nabla \times \boldsymbol{B}_t| / |\boldsymbol{B}_l|$ in the active region, where $\boldsymbol{B}_t$ and $\boldsymbol{B}_l$ are the transverse and line-of-sight components of the magnetic field in the vector magnetogram.

Except for a refinement in the measurement of L_{SS}, we use the methods described in Falconer (2001) to measure L_{SS}, I_N, and Φ and evaluate α from the active region vector magnetograms, and to estimate the uncertainties in the measured values. In Falconer (2001), L_{SS} was estimated from the pixel size and the number of pixels bracketing the strong-field, strong-shear portions of the main neutral line. In the present work, the total length of these strong-shear intervals of the main neutral line is measured more accurately by their path lengths along the zero-Gauss contour of the line-of-sight component of the magnetogram, as indicated in the example in Figure 2. (For a point on the main neutral line to be included in the length L_{SS}, the transverse field at that point must meet or surpass specified thresholds of strength and shear angle, which we have chosen to be 150 G and 45°. That is, a strong-field point qualifies for inclusion in L_{SS} if the acute angle between the observed and potential transverse field is $\geq 45°$. So, L_{SS} can be evaluated without resolution of the 180° ambiguity in the direction of the observed transverse field vector.) After resolving the 180° ambiguity in the direction of $\boldsymbol{B}_t$ as described in Falconer (2001), the net current is obtained via Ampere's law ($I_N = |\int \boldsymbol{B}_t \cdot d\boldsymbol{l}|$) by integration around a specified contour (as in Fig. 2) enclosing most of one polarity of the overall bipole. The flux content Φ is the area integral ($\int |\boldsymbol{B}_l| dA$) of the strength of the line-of-sight field over all areas of the active region in which this strength is 100 G or greater ($\geq$ twice the 1 σ noise level of 50 G in our magnetograms).

The values of our four global magnetic quantities (Φ, L_{SS}, I_N, and α) measured from each magnetogram are listed in Table 1. For each quantity, the median of its 17 measured values is given at the bottom of Table 1. Measured values that are greater than or equal to the median are shown with asterisks in Table 1, and measured values below median are shown without. This makes it easy to see in Table 1 that the active regions in our sample tend to have their four global magnetic quantities either all above median or all below median. In particular, it is obvious that the global nonpotentiality of our active regions is correlated with their size as measured by flux content.

To complete our data set, we empirically identify any CME-producing events (ejective flares) that occurred in each active region during disk passage. As in Falconer (2001), the primary observations that we use for this are the soft X-ray flux plots from *GOES* and the full-disk coronal X-ray images from *Yohkoh* SXT. As was shown by Sheeley et al. (1983), practically every *GOES* X-ray flare (C-class or stronger) that lasts for 6 hr or longer is produced together with a CME. In the SXT images, these flares have a characteristic cusped arcade structure during their long-duration decay phase, as in the example shown in Figure 1. For each long-duration ($\geq$6 hr) flare observed by *GOES* and assigned to our active region by the flare reports in Solar-Geophysical Data, we use the SXT images to confirm that the flare did occur in our active region. For shorter duration (less than 6 hr) *GOES* flares (C-class or stronger) in our active regions, if the SXT images show a cusped arcade in the decay phase of the flare, we identify that flare as a CME-producing event. For the active regions after the advent of the *SOHO* mission, from 1996 onward, whenever there are observations available from LASCO, we use these (as in Fig. 1) to verify that a CME was produced.

The last column of Table 1, for each magnetogram, lists the days (relative to the day of the magnetogram, and during disk passage of the active region) on which the active region showed evidence of having produced a CME. Like the correlation among our active region global magnetic quantities, it is obvious from inspection of Table 1 that the

CME productivity of our active regions is correlated with their global nonpotentiality.

3. RESULTS

3.1. *Correlation of Global Magnetic Quantities*

Figure 3 and Table 2 graphically display and quantify the correlation apparent in Table 1 among the four global magnetic quantities measured in our active regions. For each of the six pairs of quantities, Figure 3 shows the correlation plot of the measured values listed in Table 1. These plots confirm that each of the four quantities is positively correlated with each of the other three quantities. For each pair of quantities, Table 2 gives the number of points in each of the four quadrants defined by the two median lines in the correlation plot. The degree of correlation is determined from this 2x2 contingency table by the Fisher test (Everitt 1977), which gives the confidence level of the correlation.

The correlation confidence level from the Fisher test is expressed as a percentage: $(1 - P) \times 100\%$, where P is the probability that a correlation (i.e., inequality in population of the four quadrants) as great or greater than the observed correlation would occur by random chance. This probability is given by

$$P = \sum_{i=0}^{n} P_i, \tag{1}$$

where P_0 is the probability of the observed distribution of data points among the four quadrants occurring by random chance, and n is the number of possible distributions of the same number of data points having greater correlation than the observed distribution. For $i > 0$, P_i is the probability of one of the more highly correlated distributions occurring by random chance. The probability P_i is given by

$$P_i = \frac{(A_i + B_i)!(A_i + C_i)!(B_i + D_i)!(C_i + D_i)!}{N!A_i!B_i!C_i!D_i!}, \tag{2}$$

where A_i, B_i, C_i, and D_i are the number of points in the upper left, upper right, lower left, and lower right quadrants, and N is the total number of points:

$$N = A_i + B_i + C_i + D_i. \tag{3}$$

In our case, $N = 17$.

If $P \leq 0.05$, then the correlation has a confidence level $\geq$95% and is conventionally considered statistically significant (Everitt 1977). For a fixed distribution of data points among the four quadrants, as the number of points is increased, P decreases exponentially with the multiple m by which the number of points increases:

$$P(mA_0, mB_0, mC_0, mD_0) = [P(A_0, B_0, C_0, D_0)]^m. \tag{4}$$

For example, if (A_0, B_0, C_0, D_0) gives $P = 0.05$, then doubling the points in each quadrant $(2A_0, 2B_0, 2C_0, 2D_0)$ gives $P = (0.05)^2 = 0.0025$, and the confidence level of the correlation increases from 95% to 99.75%. On this basis, we expect significant correlations found in our present sets of 17 data points to become more significant as we sizably increase our sample of active regions.

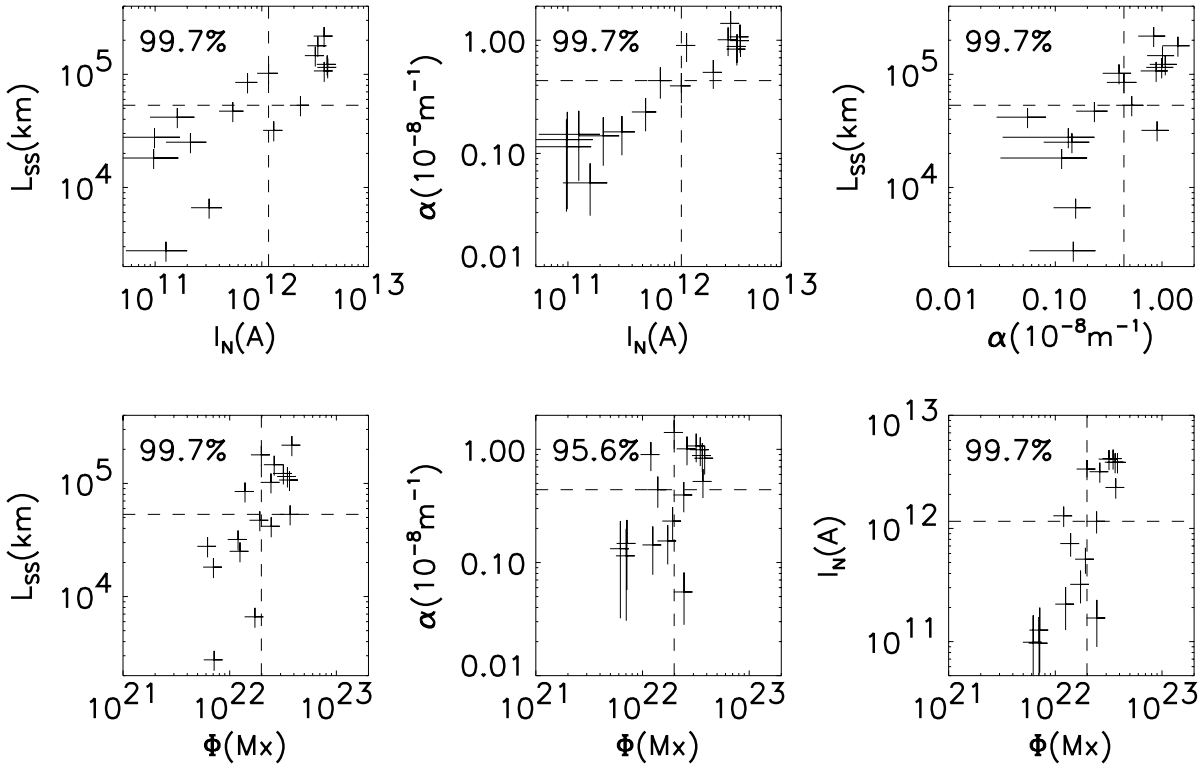

FIG. 3.—Correlation of the global magnetic quantities measured in our set of active regions. Each plot shows the correlation of one of the six different pairs of our four global magnetic quantities. Each plot has 17 data points, one for each of the 17 vector magnetograms in our set. Each data point is marked by a cross, the vertical and lateral spans of which are the measurement uncertainties. In each plot, the median of each of the two quantities is marked by a dashed line. The statistical significance of the correlation is given in the upper left corner of each plot.

TABLE 2
CORRELATION OF GLOBAL MAGNETIC MEASURES

Condition	$I_N <$ Median	$I_N \geq$ Median	Confidence Level (%)
$L_{SS} \geq$ Median...	1	8	99.7
$L_{SS} <$ Median...	7	1	
$\alpha \geq$ Median.....	1	8	99.7
$\alpha <$ Median.....	7	1	
$\Phi \geq$ Median	1	8	99.7
$\Phi <$ Median	7	1	
	$\Phi <$ Median	$\Phi \geq$ Median	
$L_{SS} \geq$ Median...	1	8	99.7
$L_{SS} <$ Median...	7	1	
$\alpha \geq$ Median.....	2	7	95.6
$\alpha <$ Median.....	6	2	
	$\alpha <$ Median	$\alpha \geq$ Median	
$L_{SS} \geq$ Median...	1	8	99.7
$L_{SS} <$ Median...	7	1	

The confidence level of the correlation of each pair of global magnetic quantities in our sample is given in Table 2 and in the corresponding plot in Figure 3. Each of the six pairs is significantly correlated. Because L_{SS}, I_N, and α are each a measure of an active region's global nonpotentiality, the strong correlation of these quantities is not surprising. Because L_{SS} and I_N are by their definitions proportional to the linear and areal size of an active region, it is also reasonable that L_{SS} and I_N should have significant correlation with the flux content Φ, which is a rough measure of the area of an active region. There is no a priori reason to expect the twist parameter $\alpha(= \mu I_N/\Phi)$ to be significantly correlated with the flux content, since dividing I_N by Φ cancels the expected Φ dependence of I_N. However, as the plot of I_N versus Φ in Figure 3 shows, in our sample of active regions the net current increases with flux content more steeply than linearly. Consequently, α shows some correlation with Φ in our sample, and it is reasonable that this correlation (confidence level 95.6%) is weaker than the correlation of I_N with Φ (99.7%). We cannot say whether the correlation of α with Φ in Figure 3 is a quirk of our particular sample, or is a true characteristic of active regions. This question begs for a larger sample of active regions.

3.2. *Correlation of the CME Productivity of our Active Regions with Their Global Magnetic Quantities*

Figures 4 and 5 and Table 3 display and quantify the other correlation that is evident in Table 1, the correlation of the CME productivity of our active regions with their global magnetic quantities. In Table 3, for each of the four global magnetic quantities, there are three contingency tables, one for each of three time windows for the production of CMEs by an active region. In each contingency table, each of the 17 magnetograms is assigned to one of the four quadrants according to whether or not the global magnetic quantity measured from the magnetogram is less than the median value and whether or not the active region produced any CMEs in the time window. With each contingency table is given the confidence level of the correlation, determined from the Fisher test. This confidence level is also given next to the axis for that quantity in the corresponding plot in Figures 4 and 5. The plots in Figure 4 are correlation plots of L_{SS} versus I_N, like those in Figure 3, showing the points for the 17 magnetograms and where they fall with respect to the medians of L_{SS} and I_N. Whether the active region produced any CMEs in the time window is shown by whether the datum cross is solid or dashed. Plots of the same format are shown in Figure 5 for Φ versus α.

The widths of the three time windows were chosen by the following rationale. A window narrower than a few days would catch few CMEs because even active regions with large global nonpotentiality seldom produce more than a few CMEs per disk passage (14 days) (Table 1). On the other hand, many active regions undergo significant evolution

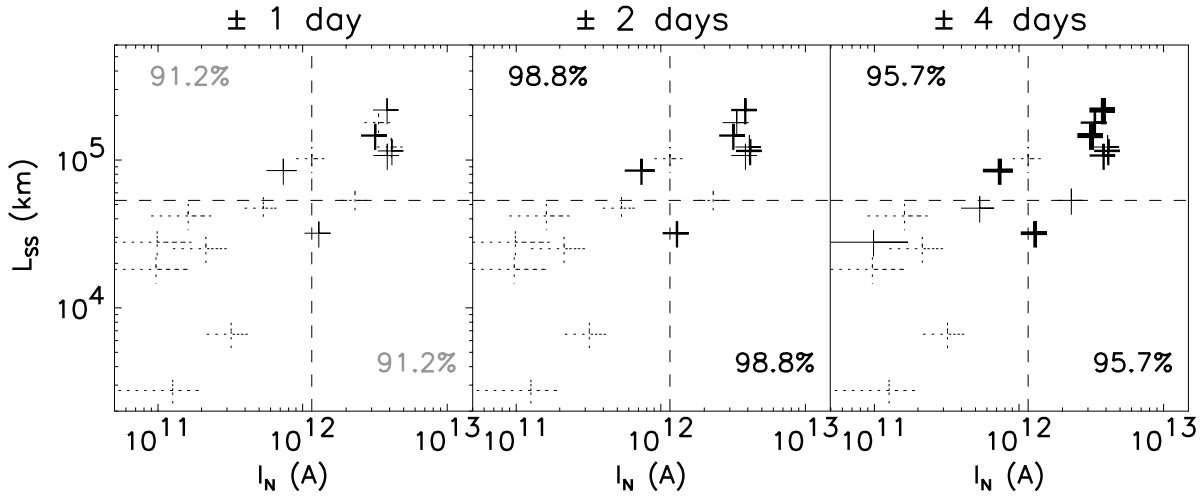

FIG. 4.—Correlation of the CME productivity of our active regions with their global nonpotentiality measures L_{SS} and I_N, for CME production within ±1 day from the day of the magnetogram (*left plot*), ±2 days (*center*), and ±4 days (*right*). Each plot shows the same 17 data points, their uncertainties, and their medians, as in Fig. 3. The crosses are dashed for active regions that produced no CMEs in the time window, solid for those that produced 1 CME, thick for 2 CMEs, and double-thick for 3 or more CMEs. For each time window, the plot shows, for L_{SS} and for I_N, that whether our active regions produced any CMEs is correlated with whether the nonpotentiality measure was above or below the median value. The significance level of this correlation for each of the two nonpotentiality measures is given near the axis for that measure.

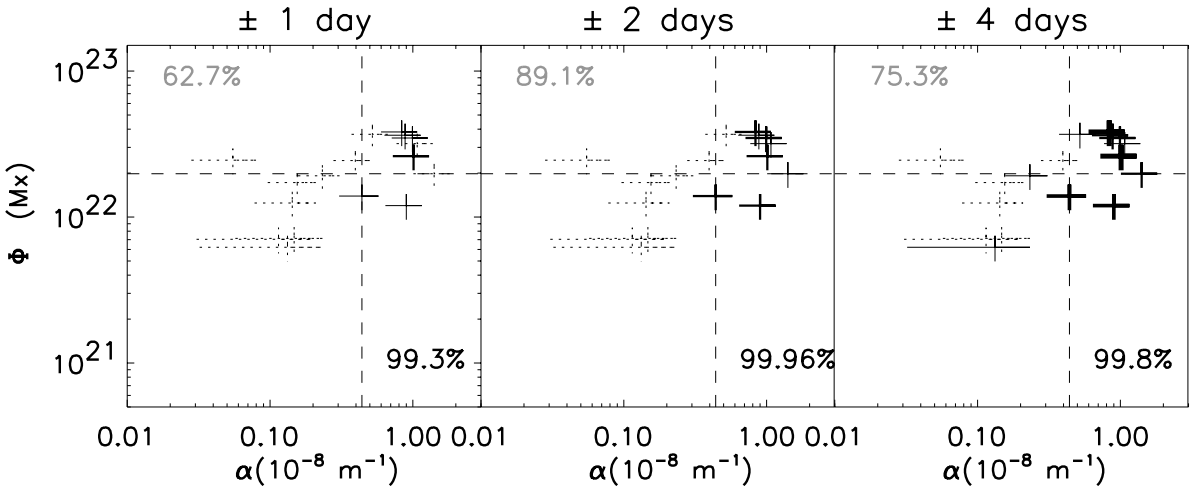

FIG. 5.—Correlation of the CME productivity of our active regions with their other two global magnetic quantities, flux content Φ, and twist parameter $\alpha(=\mu I_N/\Phi)$. These three plots have the same format as the plots in Fig. 4, and are for the same three time windows for CME production.

over the course of several days, increasing or decreasing in global nonpotentiality (e.g., active regions 7315, 8100, and 9077 in Table 1). Hence, an active region's global nonpotentiality measured on one day is not a reliable measure of the global nonpotentiality several days earlier or later. So, we expect the correlation (of a global nonpotentiality measure with whether or not the active region produced any CMEs in a time window centered on the day of the magnetogram) to increase with increasing window width for widths less than a few days, and to decrease with increasing window width beyond some width of several days. In addition, 5 days is about the time for an active region to rotate across the central face of the Sun, wherein it can produce CMEs that can hit the Earth more or less head-on. For these reasons, we chose a window spanning ±2 days from the day of the magnetogram as a roughly optimum window for assessing the promise of the global magnetic quantities for CME prediction. We added a window that is about half as wide (±1 day) and one about twice as wide (±4 days) to check whether the ±2 day window is indeed roughly optimum, i.e., gives the strongest correlation. Compatible with the above reasoning, the array of correlation confidence levels in Table 3 and Figures 4 and 5 does show for each global magnetic quantity that the correlation is stronger for the ±2 day window than for either the narrower window or the wider window.

For each of the three time windows, the correlation with CME productivity is strongest for the global twist parameter α, intermediate (and equal) for the other two measures of global nonpotentiality, L_{SS} and I_N, and weakest for the flux content Φ. For α, the correlation is statistically significant for all three windows. For L_{SS} and I_N, the correlation is significant (confidence level above 95%) for the two wider windows, and the confidence level is not far below 95% (91.2%) in the ±1 day window. In contrast, the correlation of Φ with CME productivity is less than significant in all three windows.

Because Canfield et al. (1999) have shown that CME productivity increases with active region size, we expect that the correlation of CME productivity with Φ will become statistically significant for a large enough sample of active regions. That the correlation with CME productivity in our sample is strongest for α and weakest for Φ suggests that the correlation with Φ may come mainly from the correlation of Φ with α (displayed in Table 2 and Fig. 3). A larger sample will test this possibility. If the correlation of Φ with α persists, this will indicate that at least part of the correlation of Φ with CME productivity comes from the global nonpoten-

TABLE 3
CORRELATION OF GLOBAL MAGNETIC MEASURES WITH ACTIVE REGION CME PRODUCTIVITY

	±1 DAY			±2 DAY			±4 DAY		
CONDITION	No CMEs	CMEs	Confidence Level (%)	No CMEs	CMEs	Confidence Level (%)	No CMEs	CMEs	Confidence Level (%)
$I_N \geq$ Median.....	4	5	91.2	2	7	98.8*	2	7	95.7*
$I_N <$ Median.....	7	1		7	1		5	3	
$L_{SS} \geq$ Median.....	4	5	91.2	2	7	98.8*	2	7	95.7*
$L_{SS} <$ Median.....	7	1		7	1		5	3	
$\alpha \geq$ Median.....	3	6	99.3*	1	8	99.96*	0	9	99.8*
$\alpha <$ Median.....	8	0		8	0		6	2	
$\Phi \geq$ Median	5	4	62.7	3	6	89.1	2	7	75.3
$\Phi <$ Median	6	2		6	2		4	4	

NOTE.—Asterisks denote measured values that are greater than or equal to the 95.0%.

tiality. If the correlation of Φ with α does not persist, this, together with the correlation of CME productivity with Φ, will show that the flux content (or size) of an active region has some positive influence on CME productivity independently of the global nonpotentiality.

We expect that for a larger sample of active region vector magnetograms, the confidence level of the correlation of each of the four global magnetic quantities with CME productivity will be greater than in our present sample. However, because of the small size of our sample (17 magnetograms), it remains uncertain whether the present ordering of the four quantities by strength of correlation with CME productivity will change. For the ± 2 day window, for example, Table 1 shows that for six of the magnetograms, all four global quantities are at or above median and the active region was CME productive, and for another six, all four quantities were below median and the active region produced no CMEs in the window. The differences in the confidence levels of the correlation with CME productivity come from only five active regions. Hence, it remains to be seen, as the sample of active regions is increased to twice or more its present size, whether the global twist parameter α will continue to have the strongest correlation with CME productivity, or if one of the other global quantities will turn out to be the best correlated.

4. SUMMARY AND DISCUSSION

The investigation reported here builds on the pilot study of Falconer (2001) of the usefulness of vector magnetograms for the prediction of earthward CMEs from predominantly bipolar active regions. For the present study, the data set used is expanded from Falconer's (2001) eight magnetograms of four active regions to 3 times more active regions (12) and double the magnetograms (17). From each of these active region vector magnetograms, we evaluate four global magnetic quantities: L_{SS}, the length of strong-shear strong-field main neutral line; I_N, the net current flowing up one leg of the bipole and down the other; Φ, the magnetic flux content of the active region; and $\alpha = \mu I_N/\Phi$, a flux-normalized global measure of the twist in the magnetic field. Three of these, L_{SS}, I_N, and α, are measures of the global nonpotentiality of the magnetic field of the active region, while Φ is a measure of the size of the active region. From the correlation between these quantities and from the correlation of these quantities with the observed CME productivity of the active regions, we conclude that:

1. The correlation results of the present study certify the tentative finding from the pilot study that two of the measures of global nonpotentiality, L_{SS} and I_N, are strongly correlated with each other and with the CME productivity of active regions.

2. All three of our measures of global nonpotentiality are statistically significantly correlated with each other and with the flux content.

3. For each of our four global magnetic quantities, the correlation with CME productivity is stronger for a ± 2 day time window for the CME occurrence than for windows half as wide or twice as wide. We interpret this to result from two aspects of the behavior of active regions. One is that most CME-productive active regions produce less than one CME per day. The other is that, over a time span of several days or more, active regions often undergo major changes in global nonpotentiality and/or flux content.

4. In our present sample of active regions, of the four global magnetic quantities, α is the most strongly correlated with CME productivity. For the ± 2 day window, the three measures of global nonpotentiality, L_{SS}, I_N, and α, are all significantly correlated with CME productivity, whereas the flux content Φ is correlated with CME productivity but at a less than statistically significant confidence level (less than 95%). As these differences in the strengths of correlation of the four quantities with CME productivity come from only five of our 12 active regions, a larger sample of active regions is required to establish which of the quantities, if any, is much more strongly correlated with CME productivity than the others. If, for larger samples, L_{SS} continues to have a strong correlation with CME productivity, then even if it does not have the strongest correlation, it might be the best choice for operational CME prediction, because L_{SS} can be measured from a vector magnetogram without resolution of the 180° ambiguity in the transverse field direction.

5. In the present sample, α is significantly correlated with Φ, I_N is less strongly correlated with CME productivity than is α, and the correlation of Φ with CME productivity is weaker still. If these correlations and their ordering in strength persist to larger samples, this may mean that active region size does not affect CME productivity except through global nonpotentiality.

Independent of whether active region size has a direct effect on CME productivity, the statistically significant correlation of CME productivity with our three measures of global nonpotentiality in the present sample establishes the likely usefulness of vector magnetograms for prediction of active region CMEs.

Perhaps there is some global measure of active region nonpotentiality that is still better correlated with CME productivity than is α. One possibility is the dimensionless quantity αL, where L is some characteristic length gauging the size of the active region. A convenient choice for L in our analysis would be the length of the integration contour that we use to evaluate I_N. As we expand our sample of active regions, along with L_{SS}, I_N, and α, we will examine the correlation of αL with active region CME productivity and determine which, if any, of these global nonpotentiality measures has decidedly the strongest correlation.

The validity of our results on the correlation of active region CME productivity with active region global nonpotentiality depends on the validity of our determination of the CME productivity of our active regions. The identification of a CME-producing event in an active region was primarily based on there being a C-class or stronger X-ray flare observed by *GOES*, and that *Yohkoh* SXT images showed this flare to have the cusped-arcade structure of an ejective flare. All but three of our 22 identified CME-producing events produced a long-duration ($\geq$6 hr) *GOES* flare, and the three exceptions produced a *GOES* flare that remained above background for about 3 hr. Only one of these 22 flares, a long-duration flare, had no coverage by SXT. For each of the other 21 flares there was SXT coverage, and these images showed the flare to have the cusped-arcade structure characteristic of long-duration flares. Only 12 of our 22 identified CME-producing events were covered by LASCO observations. Even though the LASCO observations show that a CME was produced in each of these cases,

strictly speaking, what we have found with the most certainty is that active regions with above-median global nonpotentiality are likely to produce long-duration ($\geq$6 hr) flares (or shorter duration flares having similar structure) and that active regions with below-median global nonpotentiality are unlikely to produce such flares. But since from Sheeley et al. (1983) it is known that any long-duration flare is nearly certain to occur in tandem with a CME, it is likely that each of our identified CME-producing events actually did produce a CME.

It is possible that we missed some CME-producing events in our active regions. All but one of the long-duration flares in our active regions had coverage by SXT, but many short-duration flares did not. If the active regions with the above-median global nonpotentiality produced more CMEs than we identified, the correlation of CME productivity with global nonpotentiality would either not change or be strengthened. Of more concern, the degree of correlation would be reduced from what we found if active regions with below-median global nonpotentiality had CME events that we missed. Sheeley et al. (1983) found that CMEs are often produced together with *GOES* X-ray flares that last for only 2–4 hr. Many more *GOES* flares of such short duration occurred in our active regions than did *GOES* flares of long duration. Most of these short-duration flares were in the active regions of above-median global nonpotentiality, but many were in the below-median active regions. Most of the short-duration flares in our active regions were observed by SXT, and only three of these showed structure characteristic of ejective flares; the rest all appeared to be confined flares. (See Moore et al. [2001] for examples of the coronal X-ray structure of long-duration ejective flares and the distinctly different structure of confined flares.) On this basis, we assumed that only three of the short-duration flare events in our active regions produced a CME.

While it is possible that some of the short-duration flares missed by SXT were CME-producing events, from the following considerations, we think that very few were. Many of the short-duration flares that Sheeley et al. (1983) found to occur together with a CME may not have been the eruptive event (magnetic explosion) that produced the CME. It is known that CMEs that arise from filament-eruption events in quiet regions often trigger, or are triggered by, a flare in an active region near one end of the erupting filament (e.g., Machado et al. 1988; Kahler 1992). So, it may be that most active region short-duration flares that occur in near synchrony with a CME are confined flares, do not have cusped-arcade structure, and are not the event that produced the CME (which in this case is seated outside the active region). In addition, because each of our active regions was predominantly bipolar, they might be expected to have had few short-duration flares that produced CMEs. Sterling & Moore (2001) present three homologous short-duration flares that were each produced together with a CME. In this case, the overall active region had a complex multipolar structure, and these flares were seated on a secondary neutral line in compact emerging flux on the trailing edge of a large sunspot at the trailing end of the active region. In our active regions, most of the short-duration flares that were observed by SXT occurred on the main neutral line in the interior of the overall bipole of the active region, and all but three appeared to be confined rather than ejective. These observations suggest that very few short-duration flares in bipolar active regions are CME-producing events.

For the above reasons, while some of the short-duration flares in our active regions had no coverage by SXT, we think that it is unlikely that more than one or two of these produced a CME. That is, we are fairly confident that we missed few if any CME-producing events that produced C-class or stronger *GOES* X-ray flares in our active regions.

The improved method of measuring L_{SS} was devised in collaboration with Neil Griffith and George Fisher. We thank the referee for pointing out that αL might be more strongly correlated with CME productivity than is α. The research reported in this paper was supported by funding from NSF's Division of Atmospheric Sciences through its Space Weather program and by funding from NASA's Office of Space Science through the Living With a Star program and the Solar Physics Supporting Research and Technology program of its Sun-Earth Connection theme.

REFERENCES

Antiochos, S. K., Dahlburg, R. B., & Klimchuk, J. A. 1994, ApJ, 420, L41
Canfield, R. C., Hudson, H. S., & McKenzie, D. 1999, Geophys. Res. Lett., 26, 627
Everitt, B. S. 1977, The Analysis of Contingency Tables (London: Chapman & Hall)
Falconer, D. A. 2001, J. Geophys. Res., 106, 25185
Falconer, D. A., Gary, G. A., Moore, R. L., & Porter, J. G. 2000, ApJ, 528, 1004
Gosling, J. T. 1996, ARA&A, 34, 35
Hagyard, M. J., Cumings, N. P., West, E. A., & Smith, J. E. 1982, Sol. Phys., 80, 33
Kahler, S. 1987, Rev. Geophys., 25, 663
Kahler, S. W. 1992, ARA&A, 30, 113
Krimigis, S. M. 1992, in The Astronomy and Astrophysics Encyclopedia, ed. S. P. Maran (New York: Van Nostrand Reinhold), 332
Machado, M. E., Moore, R. L., Hernandez, A. M., Rovira, M. G., Hagyard, M. J., & Smith, J. B., Jr. 1988, ApJ, 326, 425
MacQueen, R. M., & Fisher, R. R. 1983, Sol. Phys., 89, 89
Moore, R. L. 1987, Sol. Phys., 113, 121
———. 1988, ApJ, 324, 1132
———. 2001, in Encyclopedia of Astronomy and Astrophysics (Bristol: Instit. of Phys. Publ.)
Moore, R. L., Hagyard, M. J., & Davis, J. M. 1987, Sol. Phys., 113, 347
Moore, R. L., Hagyard, M. J., Davis, J. M., & Porter, J. G. 1991, in Flare Physics in Solar Activity Maximum 22, ed. Y. Uchida et al. (Berlin: Springer), 324
Moore, R. L., & Roumeliotis, G. 1992, in Eruptive Solar Flares, ed. Z. Svestka, B. V. Jackson, & M. E. Machado (Berlin: Springer), 69
Moore, R. L., Schmieder, B., Hathaway, D. H., & Tarbell, T. D. 1997, Sol. Phys., 176, 153
Moore, R. L., Sterling, A. C., Hudson, H. S., & Lemen, J. R. 2001, ApJ, 552, 833
Reames, D. V. 1999, Space Sci. Rev., 90, 413
Rust, D. M., et al. 1980, in Solar Flares, ed. P. A. Sturrock (Boulder: Colorado Associated Univ. Press), 273
Sheeley, N. R., Jr., Howard, R. A., Koomen, M. J., & Michels, D. J. 1983, ApJ, 272, 349
Sterling, A. C., & Moore, R. L. 2001, J. Geophys. Res., 106, 25227
Tandberg-Hanssen, E., Martin, S. F., & Hansen, R. T. 1980, Sol. Phys., 65, 357
Tsuneta, S., et al. 1991, Sol. Phys., 136, 37
Wagner, W. J. 1984, ARA&A, 22, 267
West, E. A., Hagyard, M. J., Gary, G. A., Smith, J. E., Adams, M., & Cloyd, R. 2002, Proc. SPIE, 4481, 270
Zirin, H., & Tanaka, K. 1973, Sol. Phys., 32, 173